

Electron Doping of Cuprates via Interfaces with Manganites

S. Yunoki, A. Moreo, and E. Dagotto

*Department of Physics and Astronomy, The University of Tennessee, Knoxville, Tennessee 37996, USA and
Materials Science and Technology Division, Oak Ridge National Laboratory, Oak Ridge, Tennessee 32831, USA.*

S. Okamoto and S. S. Kancharla

Materials Science and Technology Division, Oak Ridge National Laboratory, Oak Ridge, Tennessee 32831, USA.

A. Fujimori

Department of Physics, University of Tokyo, 7-3-1 Hongo, Bunkyo-ku, Tokyo 113-0033, Japan.

(Dated: November 5, 2018)

The electron doping of undoped high- T_c cuprates via the transfer of charge from manganites (or other oxides) using heterostructure geometries is here theoretically discussed. This possibility is mainly addressed via a detailed analysis of photoemission and diffusion voltage experiments, which locate the Fermi level of manganites above the bottom of the upper Hubbard band of some cuprate parent compounds. A diagram with the relative location of Fermi levels and gaps for several oxides is presented. The procedure discussed here is generic, allowing for the qualitative prediction of the charge flow direction at several oxide interfaces. The addition of electrons to antiferromagnetic Cu oxides may lead to a superconducting state at the interface with minimal quenched disorder. Model calculations using static and dynamical mean-field theory, supplemented by a Poisson equation formalism to address charge redistribution at the interface, support this view. The magnetic state of the manganites could be antiferromagnetic or ferromagnetic. The former is better to induce superconductivity than the latter, since the spin-polarized charge transfer will be detrimental to singlet superconductivity. It is concluded that in spite of the robust Hubbard gaps, the electron doping of undoped cuprates at interfaces appears possible, and its realization may open an exciting area of research in oxide heterostructures.

PACS numbers: 73.20.-r, 74.78.Fk, 73.40.-c

INTRODUCTION

The study of oxide heterostructures is rapidly developing into one of the most promising areas of research in strongly correlated electronic systems. The current excitement in this field was in part triggered by the recent discovery of conducting interfaces, with a substantial high carrier mobility, between two insulating perovskites [1, 2]. These results were obtained by growing abrupt layers of the insulators $\text{LaTi(3+)}\text{O}_3$ and $\text{SrTi(4+)}\text{O}_3$. When the spatial distribution of the extra electron was observed with an atomic-scale electron beam, it was found to correspond to a metallic state at the interface [1]. Theoretical investigations of these systems [3, 4, 5], using Hartree-Fock and DMFT techniques, concluded that the leakage of charge from one layer to the other explains the results. Thus, charge transfer between materials in heterostructures can be used to stabilize interface states that otherwise would only be obtained via the chemical doping of the parent oxide compound. This last procedure has the concomitant effect of introducing quenched disorder into the sample. Then, for the preparation of doped materials without the extra complication of disorder, for the realization of two-dimensional versions of perovskites, and for the exploration of “oxide electronics” devices and functionalities, the experimental and theoretical analysis of oxide heterostructures is a promising and vast field, and

its study is only now starting [6, 7, 8].

Before the recent developments mentioned above, ferromagnetic/superconducting (FM/SC) heterostructures had already received considerable attention. The analysis of spin injection from a ferromagnetic material to an electrode is of much importance for further progress in the area of spintronics. Other properties of interest in FM/SC heterostructures include: (i) spin-mixing effects that can induce spin-triplet pairing correlations at the interface [9]; (ii) Josephson couplings between two singlet-superconducting layers separated by a half-metallic ferromagnet [10]; (iii) oscillations in the singlet pairing amplitude detected in SC/FM/SC geometries [11]; and (iv) magnetic exchange coupling in FM/SC/FM geometries [12, 13]. Since transition metal oxides have similar lattice spacings, the combination of colossal magnetoresistance (CMR) manganites [8, 14, 15] and high- T_c cuprates has been specially investigated [16, 17, 18]. Experimental results suggest a strong FM/SC interplay resulting in the injection of spin polarized carriers into the SC layers [12]. Of particular importance for the purposes of our investigations, the transfer of charge from the $\text{La}_{1-x}\text{Ca}_x\text{MnO}_3$ (LCMO) ferromagnet to the $\text{YBa}_2\text{Cu}_3\text{O}_y$ (YBCO) superconductor has been observed in recent experiments using EELS techniques [19]. In this case, the addition of electrons, namely the suppression of holes, in the YBCO component led to the concomitant suppression of super-

conductivity and a transition to an insulating state. Similar effects are also believed to occur in grain boundaries of superconductors [20]. In other LCMO/YBCO superlattice setups, the superconducting critical temperature was also found to be suppressed [21]. This may be caused by the influence of spin-polarized carriers moving from LCMO to YBCO, breaking singlet Cooper pairs, or by the reduction of the number of hole carriers [19], or both.

It is the main purpose of the investigation reported here to analyze whether the previously observed electronic charge transfer at interfaces from manganites, such as LCMO or $\text{La}_{1-x}\text{Sr}_x\text{MnO}_3$ (LSMO), to hole-doped cuprates, such as YBCO, can be extended to the case where the cuprate is in an undoped state. If this still occurs, namely if estimations of work functions lead us to believe that the Fermi level of the manganite remains above the first empty states of the undoped cuprate, then this Cu oxide will receive an excess of electrons, leading to the *electron doping* of an antiferromagnetic (AF) state at heterostructure interfaces [22]. This mixing of cuprates and manganites could lead either to (i) a metallic spin-polarized state at the interface, if the manganite is ferromagnetic, or to (ii) an electron-doped superconductor at low enough temperatures, if the spin polarization is not strong enough to destroy Cooper pairs or if the manganite used is not ferromagnetic. This mechanism would allow for the electronic doping of a parent cuprate compound without the complication of the Coulombic and structural disorder introduced by chemical doping. The fact that this is electron doping, as opposed to the already investigated interfacial hole doping, is particularly interesting since a variety of material issues has prevented the electron-doped branch of high- T_c superconductors to develop as vastly as those that are hole doped.

Once again, note that if the manganite is ferromagnetic, then the charge transfer to the undoped cuprate would occur via polarized electrons, which suppress spin singlet superconductivity. Thus, there are two *competing* tendencies: adding electrons favors superconductivity, but its spin polarization suppresses it. The outcome is difficult to predict. Recent investigations using realistic microscopic models focusing on a manganite/insulator interface predict that a complex pattern of phase separation between FM and AF regions could occur [23]. Thus, even if superconductivity is not induced, the resulting state would be interesting, due to the interplay between ferro and antiferromagnetic tendencies. More importantly, note that the manganite involved in the heterostructure does *not* need to be ferromagnetic: low-bandwidth Mn oxides present a wide variety of spin/charge/orbital order states, other than ferromagnetism [14, 15]. Even large-bandwidth manganites have non-FM states at small and large enough hole concentration. Thus, inducing a SC state is a real possibility with the proper choice of the manganite partner to the cuprate.

A qualitative representation of the transfer of charge is shown in Fig. 1 for the cases of a doped cuprate, such as discussed in [19], and for an undoped cuprate, the focus of our investigation reported below. In case (a), SC is destroyed, while in the proposed case (b), SC is induced (if the manganite is not ferromagnetic). Our main result is that the novel scenario (b) appears possible. Our conclusion is based on (i) a detailed analysis of the work functions of the materials of relevance for these investigations, mainly involving the study of photoemission and diffusion voltage published data, as well as (ii) rough calculations at the mean-field and dynamical mean-field levels, showing that there is no fundamental problem preventing superconductivity from happening at the interface. However, it must be clearly expressed that our contribution should be considered as only the first theoretical steps toward realizing electron doping at cuprate interfaces, and considerable more work remains to be carried out. For instance, issues such as lattice reconstructions and polarity of the involved interfaces have *not* been analyzed here (only electronic reconstructions at idealized perfect interfaces were investigated). Vacancies and the most optimal location of oxygens at the interface have not been investigated as well. However, even with these caveats we believe the conclusions described below are sufficiently interesting that they deserve experimental efforts to attempt their realization in real heterostructures.

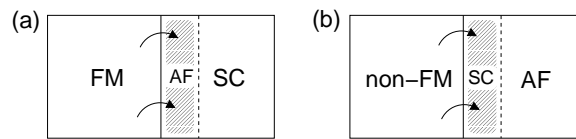


FIG. 1: Schematic representation of the systems studied here. (a) is a heterostructure involving a ferromagnetic (FM) half-metal system, such as LCMO, and a superconductor (SC), such as YBCO. In this case, an antiferromagnetic (AF) insulating state is induced at the interface. (b) is a heterostructure involving a non-FM manganite and an undoped AF cuprate. Here, the transfer of charge may lead to a superconducting state at the interface. Arrows indicate the direction of flow of electrons, which are accumulated in the gray region.

The organization of the manuscript is as follows: first, we carry out a detailed analysis of available experimental information to judge if the Fermi level of manganites is above the lowest-energy empty state of several undoped cuprates. This is described in detail, because it provides a systematic procedure to address other oxide heterostructures in the future. Second, a model calculation in the mean-field approximation is carried out, both for static and dynamical cases. No fundamental problem is found with the proposal of having superconductivity induced at the manganite/cuprate interface. The paper concludes with a discussion and summary.

ESTIMATION OF OXIDES CHEMICAL POTENTIAL DIFFERENCES USING PHOTOEMISSION AND DIFFUSION VOLTAGE EXPERIMENTS

Overview

For the success of the emergent field of oxide heterostructures it is crucial to properly determine the relative work functions of the materials involved, since these work functions control the curvature of the valence and conduction bands (VB and CB) of the constituent materials, and ultimately the carrier concentration at the interfaces. Work functions of conventional metals and semiconductors have been studied for decades establishing the fundamental background for current electronics. Thus, for the next-generation electronic devices utilizing the complex properties of correlated-electron systems, such as high- T_c cuprates and CMR manganites, determining the relative work functions of a variety of transition-metal oxides is equally important.

Photoemission spectroscopy (PES) is an important technique in this context. PES has provided fundamental information to uncover the properties of complex oxides. However, although PES techniques can be of considerable help for oxide heterostructures, only a limited number of experiments have been reported specifically addressing the work function of transition-metal oxides [24].

By measuring the diffusion voltage V_d (or built-in potential) of a junction between two materials of interest, one can also extract the chemical potential differences between them. This diffusion voltage is the potential barrier at the interface after the rearrangement of charge occurs. If there are no extra contributions to V_d , such as those caused by interface polarities, impurities, or lattice reconstructions, then V_d is equivalent to the work function difference between the two constituents. If the work function of one of the materials is known, the work function of the other can be estimated. This provides another procedure to study the band alignment of oxides.

The purpose of this section is to provide a rough estimation of the band diagram of perovskite transition-metal oxides (cuprates and manganites) using the experimental data currently available. This is achieved by combining information from chemical potential shifts obtained using PES with diffusion voltage measurements on heterostructures.

Parent compounds of High- T_c cuprates

Since the discovery of high- T_c superconductivity in the cuprates, considerable experimental information has been accumulated about these compounds. In particular, the chemical-potential jump from the hole-doped to the electron-doped materials has been one of the important

topics since it is closely related to the Mott/Hubbard (or charge transfer) gap. Here, let us first consider La_2CuO_4 (LCO) and Nd_2CuO_4 (NCO) as the parent compounds of hole-doped and electron-doped cuprates, respectively. It should be mentioned that these compounds have different structures: LCO has the layered perovskite or $n = 1$ Ruddlesden-Popper structure, while NCO presents the so-called T' -structure without apical oxygen. Even though the electronic properties of the CuO_2 planes are quite similar for LCO and NCO, the different overall structures suggest that small differences may exist in their chemical potentials, as discussed below.

From the optical measurements, it has been suggested that the chemical potential of LCO is located 0.4 eV above the top of the valence band [25]. Similar results were obtained with PES techniques [26]. Polaronic effects are believed to be the cause of this somewhat “mysterious” shift between the top of the valence band and the actual location of the chemical potential in LCO [27]. Similarly, resonant-photoemission studies on NCO revealed that the chemical potential of NCO is located 0.7 eV above the valence band [28, 29]. If the positions of the valence bands are identical between LCO and NCO, then their chemical potential jump becomes $0.7 - 0.4 = 0.3$ eV [30]. Although an accurate determination of the individual chemical potentials of these materials remains to be done, estimations based on the shifts of the O 1s and Cu 2p core levels indicate that the chemical potential jump is at most 0.5 eV [31]. Then, the positions of the valence bands can be assumed to be the same, although with a $\lesssim 0.2$ eV uncertainty.

To complete the band diagram, information about the location of the unoccupied conduction, or upper Hubbard band, is needed. From optical spectroscopy, it was first suggested that the Mott gaps of LCO and NCO are about 2 eV and 1.5 eV, respectively [32]. However, numerical studies of the Hubbard model on finite-size clusters using appropriate hopping amplitudes for the cuprates revealed that the Mott gap in Cu oxides was in fact an indirect one [33]: the top of the lower-Hubbard band is at momenta $(\pm\pi/2, \pm\pi/2)$ while the bottom of the upper-Hubbard band lies at $(\pi, 0)$ and $(0, \pi)$. Thus, the Mott gap is indirect and smaller than the optical gap. The indirect nature of this gap has been confirmed by a recent resonant x-ray study [34]. Considering the ratio between the magnitudes of direct gap and indirect gap from the theoretical considerations and the optical gap obtained by the experiments, the separation between the VB and CB of LCO and NCO is estimated to be about 1.5 eV and 1 eV, respectively [35]. Combining all this information together, the schematic band diagram for these materials can be constructed and it is shown in Fig. 2.

Next, let us address another series of high- T_c cuprates: YBCO. The diffusion voltage of the heterostructure between YBCO (oxygen contents unclear) and 0.05wt% Nb-doped SrTiO_3 (STO) ($\text{Nb}_{0.05}\text{-STO}$) has been measured

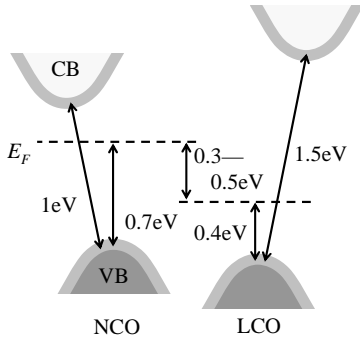


FIG. 2: Schematic band diagrams of NCO and LCO [31] based on the chemical potential jump between NCO and LCO found in a resonant-photoemission study [29], revised by considering the recent discovery of an indirect Mott gap in the cuprates [34]. Chemical potentials (dashed lines) of NCO and LCO are located about 0.7 eV and 0.4 eV above the valence bands, respectively. Note that the top of the valence bands of NCO and LCO do not necessarily match, but estimations discussed in the text locate them very close to one another. There remains an ambiguity in the chemical potential jump between these two materials, but it is believed to be at most 0.5 eV [31]. For more details see text.

[36]. The chemical potential of YBCO was found to be 1.5 eV below that of $\text{Nb}_{0.05}\text{-STO}$.

To establish a connection with the single-layer cuprates, note that similar experiments on the diffusion voltage of the single-layer parent compound Sm_2CuO_4 (SCO) and 0.01wt% Nb-doped SrTiO_3 ($\text{Nb}_{0.01}\text{-STO}$) have been very recently performed [37]. SCO is an isostructural material of NCO, with the same T' -structure and formal valences, therefore NCO is expected to have a chemical potential very similar to that of SCO. The recent experiments of Nakamura *et al.* revealed that the chemical potential of SCO is 1.3 eV below that of $\text{Nb}_{0.01}\text{-STO}$ [37]. Although there is a slight difference in the doping concentration of Nb used for the two experiments (0.05wt% Nb for YBCO and 0.01wt% for SCO), by reducing the Nb concentration to 0.01wt% the diffusion voltage is expected to increase only by 0.1 eV or less because of band-gap narrowing effects [38]. Thus, by combining the diffusion voltages on SCO- and YBCO-based heterostructures involving a Nb-doped STO substrate, the chemical potential of SCO is estimated to be $\sim 1.5 + 0.1 - 1.3 = 0.3$ eV above that of YBCO.

Furthermore, assuming that the behavior of SCO and NCO are identical, based on the similarity of their structures, then the chemical potential of LCO can be estimated by considering the chemical potential jump between NCO and LCO. Figure 3 summarizes the band diagram for the various high- T_c cuprates studied here. From these results, it is deduced that the parent compounds of hole-doped cuprates have fairly similar chemical potentials despite their different crystal structures.

Doping dependence of the chemical potential in High- T_c cuprates

The doping dependence of the chemical potential is important when using doped compounds for the oxide heterostructures. The chemical potential shifts from their parent compounds of various high- T_c cuprates have been intensively studied [29, 41, 42, 43]. For the benefit of the readers, the main results are summarized in Fig. 4 (a) for hole-doped compounds, and Fig. 4 (b) for electron-doped compounds [44].

There are still considerable discussions on the electronic properties of the underdoped region of $\text{La}_{2-x}\text{Sr}_x\text{CuO}_4$ (LSCO), involving concepts such as stripe formation, phase separation, and spin glass. Those may explain the flat chemical potential shifts of LSCO at $0 \leq x < 0.15$. However, focusing on the overdoped region where the mixed-phase complexity is reduced, then the chemical potential shifts behave linearly with hole doping with a slope of about 0.2 eV per 0.1 carrier concentration, which is close to that of electron-doped $\text{Nd}_{2-x}\text{Ce}_x\text{CuO}_4$ (NCCO). This may indicate that the band structures of the CuO_2 planes in those compounds are similar, as widely believed. On the other hand, the $\Delta\mu$ vs. carrier concentration slope for $\text{Bi}_2\text{Sr}_2\text{CaCu}_2\text{O}_{8+y}$ (Bi2212) is larger than for the single-layer compounds, perhaps due to its bilayered nature.

Connecting the High- T_c cuprates with the CMR manganites

As already discussed, both from the fundamental physics as well as the device engineering perspective, heterostructures involving high- T_c cuprates and CMR manganites are important. Here, we consider the cubic perovskite manganites first, and then turn to the double-layered manganites.

It should be mentioned that the *direct* measurement of the work function of cubic manganites has been performed by several groups using PES [45, 46] and the Kelvin method [47], and results are approximately consistent with one another indicating an intrinsic work function ~ 4.8 eV for $\text{La}_{1-x}\text{Sr}_x\text{MnO}_3$ with $x = 0.3, 0.4$. These experimental data are important in considering interfaces with the cuprates. However, as the individual work functions of many cuprates are not yet available but only their differences, then we have to consult other experiments in order to establish a connection between manganites and cuprates. Here, we consider PES experiments that measured the chemical potential shift in doped manganites [40], and those that provided the diffusion-voltage on $\text{La}_{0.8}\text{Sr}_{0.2}\text{MnO}_3$ (20% hole-doped LSMO)/ $\text{Nb}_{0.05}\text{-STO}$ heterostructures [39].

According to the experiment by Matsuno *et al.* [40], the chemical potential of $\text{La}_{1-x}\text{Sr}_x\text{MnO}_3$ (LSMO)

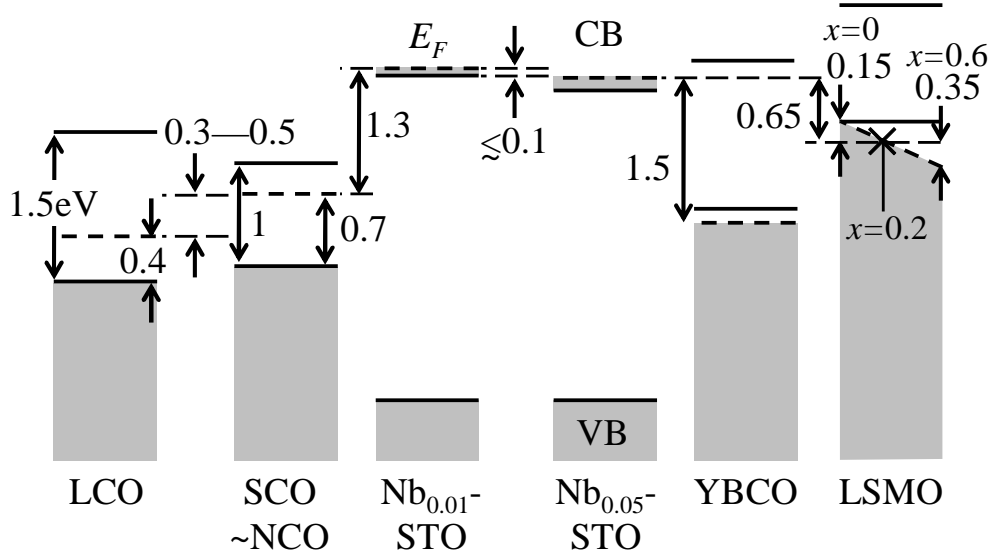


FIG. 3: Schematic band diagrams of LCO, SCO(NCO), $\text{Nb}_{0.01}\text{-STO}$, $\text{Nb}_{0.05}\text{-STO}$, YBCO, and LSMO based on diffusion voltage measurements [36, 37, 38, 39] and photoemission spectroscopy [29, 31, 40]. Tops of valence bands (VB) and bottoms of conduction bands (CB) are indicated by solid lines, while chemical potentials are indicated by dashed lines.

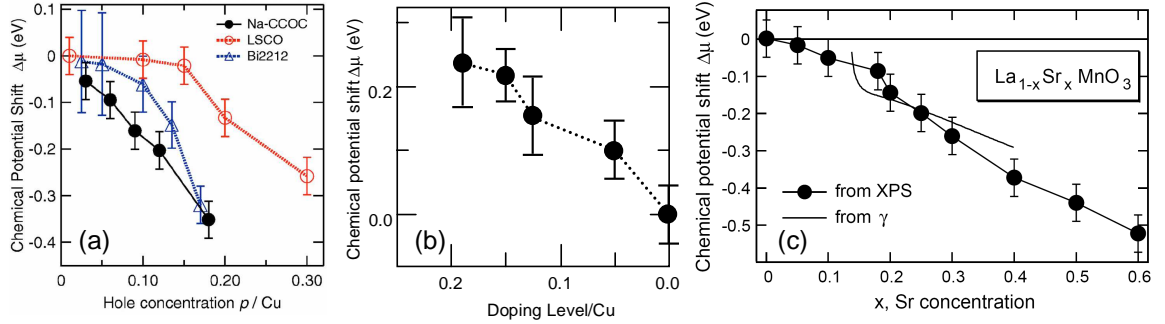


FIG. 4: Chemical-potential shifts of various transition-metal oxides, reproduced from photoemission experiments. (a) are the results for hole-doped cuprates. Na-CCOC: $\text{Ca}_{2-x}\text{Na}_x\text{CuO}_2\text{Cl}_2$ [43], LSCO: $\text{La}_{2-x}\text{Sr}_x\text{CuO}_4$ [41], and Bi2212: $\text{Bi}_2\text{Sr}_2\text{Ca}_{1-x}\text{R}_x\text{Cu}_2\text{O}_{8+y}$ ($\text{R}=\text{Pr}, \text{Er}$) [42]. The absolute values at the undoped origin of each series are assumed to be the same. Reproduced from [43]. (b) Chemical potential shift of electron-doped cuprates NCCO: $\text{Nd}_{2-x}\text{Ce}_x\text{Cu}_2\text{O}_4$. Reproduced from [44]. (c) Chemical-potential shift of LSMO. These shifts are measured at liquid-nitrogen temperature except for LaMnO_3 . Reproduced from [40].

changes rather monotonically from the parent compound LaMnO_3 to a value $\Delta\mu = -0.5$ eV for $\text{La}_{0.4}\text{Sr}_{0.6}\text{MnO}_3$ (60% hole-doped LSMO) (see Fig. 4 (c)). Furthermore, diffusion voltage measurements on a $\text{La}_{0.8}\text{Sr}_{0.2}\text{MnO}_3$ (20% hole-doped LSMO)/ $\text{Nb}_{0.05}\text{-STO}$ heterostructure, done by Muramatsu *et al.* [39], reported a value $V_d = 0.65$ eV. Combining these experiments, the bands of LSMO can be aligned relative to those of the cuprates obtained in the previous section. Figure 3 summarizes the band alignment of cuprates and manganites, which is our main result of this section. In particular, the chemical potential shifts between the various cuprates of potential relevance and the 20% doped LSMO are summarized as

follows: (i) for SCO $\Delta\mu = \mu_{\text{LSMO}} - \mu_{\text{SCO}} \sim 0.55$ eV, (ii) for LCO $\Delta\mu = \mu_{\text{LSMO}} - \mu_{\text{LCO}} \sim 0.85\text{--}1.05$ eV, and (iii) for YBCO $\Delta\mu = \mu_{\text{LSMO}} - \mu_{\text{YBCO}} \sim 0.85$ eV. In particular, it is natural to expect that electrons be transferred from LSMO to the valence band of hole-doped YBCO at an interface between the two materials. This has already been observed experimentally [19], thus it is reassuring that the simple procedure followed here is consistent with available experimental information [48].

Consider now another class of Mn oxides, the double-layered manganites with the so-called $n = 2$ Ruddlesden-Popper structure. Direct measurements of work function using photoemission have actually been performed on

$\text{La}_{1.2}\text{Sr}_{1.8}\text{Mn}_2\text{O}_7$. It has been reported that the work function of $\text{La}_{1.2}\text{Sr}_{1.8}\text{Mn}_2\text{O}_7$ increases with decreasing temperature across the Curie temperature (125 K) from ~ 3.5 eV at 180 K to ~ 3.56 eV at 60 K [24], while the simple double-exchange model predicts the opposite trend. This fact may indicate the importance of several ingredients neglected in the double-exchange model, such as electron-electron interaction, electron-lattice interaction, and orbital degeneracy. The important point worth emphasizing here is that the work function of the double-layered manganite is more than 1 eV smaller than that of cubic LSMO (whose work function is ~ 4.8 eV) [45, 46, 47], which means that the chemical potential of the double-layer manganite is more than 1 eV *higher* than the cubic perovskite LSMO. Thus, at least naively, it should be possible to inject electrons to the undoped cuprates using the double-layer manganites. However, there are issues that remain to be clarified for this conclusion to be valid, particularly the role of the surface condition: for double-layered manganites, the cleaved surface used in PES experiments is always AO^{2-} (A: A-site ion, such as La^{3+} and Sr^{2+}), thus positively charged. The low work function of bilayered manganites could be caused by this charged surface. On the other hand, for cubic manganites the surface can be either positively charged (AO termination) or negatively charged (MnO_2 termination). For this purpose, photoemission experiments on cubic manganites with controlled surface conditions are highly desirable.

Summarizing, in this subsection we discussed the possible electron doping of cuprates from manganites at ideal interfaces. In the paragraphs above, it was concluded that the parent compounds of electron-doped cuprates, such as NCO and SCO, are the best candidates for this purpose since they have the lowest conduction band (the CB in LCO is about 0.5 eV higher than that in NCO, and the CB in YBCO is expected to be even higher than those of NCO and LCO). To dope electrons into a cuprate parent compound, the minimal condition is that the chemical potential of manganites be higher than the bottom of the conduction band (or the chemical potential if they are not the same) of the undoped cuprate involved. This condition seems to be satisfied for cubic manganites LSMO in a substantial doping range x that includes FM and AF states, when mixed with NCO or SCO [49]. Possible improvements may be achieved by using double-layered manganites, which have about 1 eV higher chemical potential than cubic manganites.

SUPERCONDUCTIVITY AT THE MANGANITE/CUPRATE INTERFACE: STATIC MEAN-FIELD APPROXIMATION

The simple ideas described in the previous sections on the possibility of electron doping of cuprates at interfaces

need to be checked in more theoretical detail to confirm their consistency. For this purpose, first a static mean-field study will be here discussed, followed in the next section by a more detailed analysis including dynamical effects. The emphasis will be given to a manganite/cuprate interface, but the generation of superconductivity by electron doping can occur for any other combination where electrons are donated to the cuprates.

The model used here is defined by the following Hamiltonian on a three-dimensional cubic lattice:

$$H = - \sum_{\mathbf{i}, \mathbf{j}} \sum_s t_{\mathbf{ij}} c_{\mathbf{i}s}^\dagger c_{\mathbf{j}s} + H_I + \sum_{\mathbf{i}} (\phi_{\mathbf{i}} - \mu + W_{\text{L/R}}) n_{\mathbf{i}}. \quad (1)$$

Here $c_{\mathbf{i}s}^\dagger$ is the electron creation operator at site $\mathbf{i} = (i_x, i_y, i_z)$ with spin $s = \uparrow, \downarrow$, $n_{\mathbf{i}}$ is the electron density at site \mathbf{i} , and $t_{\mathbf{ij}}$ is the nearest-neighbor hopping, which is t on the xy plane and t_z in the z direction. $\phi_{\mathbf{i}}$ is the electronic potential (discussed in more detail later) that will take into account effects related to the charge redistribution. μ is the chemical potential, and W_{L} (W_{R}) are site potentials for the left (right) side of the system to regulate the transfer of charge. H_I contains the interaction terms. On the left side of the system (the manganite) the interaction is

$$H_I^{(\text{L})} = -J_{\text{H}} \sum_{\mathbf{i}} \sum_{\alpha, \beta} c_{\mathbf{i}\alpha}^\dagger (\vec{\sigma})_{\alpha\beta} c_{\mathbf{i}\beta} \cdot \vec{S}_{\mathbf{i}}, \quad (2)$$

which is the standard “double-exchange” term. $\vec{\sigma} = (\sigma_x, \sigma_y, \sigma_z)$ are Pauli matrices, and $\vec{S}_{\mathbf{i}}$ is a classical localized spin at site \mathbf{i} ($|\vec{S}_{\mathbf{i}}| = 1$) representing the t_{2g} spins. On the right side of the system, the cuprate, the standard repulsive Hubbard interaction ($U > 0$) is supplemented by a nearest-neighbors attraction ($V < 0$) that favors superconductivity in the d -wave channel:

$$H_I^{(\text{R})} = U \sum_{\mathbf{i}} n_{\mathbf{i}\uparrow} n_{\mathbf{i}\downarrow} + V \sum_{\langle \mathbf{ij} \rangle} n_{\mathbf{i}} n_{\mathbf{j}}. \quad (3)$$

The number operator is $n_{\mathbf{i}s} = c_{\mathbf{i}s}^\dagger c_{\mathbf{i}s}$, and $\langle \mathbf{ij} \rangle$ indicates a pair of nearest-neighbor sites \mathbf{i} and \mathbf{j} on the xy plane. It is well known that this t - U - V model leads to a rich phase diagram, that includes superconductivity [50]. Periodic (open) boundary conditions are used in the x and y (z) directions for a lattice of size $L = L_x \times L_y \times L_z$ sites. The focus of the results described below is on $L_x = L_y = 16$, but other sizes have been checked confirming that size effects are not strong in this study.

Two comments are in order: (1) A fully realistic model for manganites should contain two e_g -orbitals and a Jahn-Teller electron-phonon coupling. However, it is common practice in this context to use just one e_g -orbital for simplicity, since several phenomena are common to both one and two orbitals [14]. Moreover, the focus here is not on the CMR regime but only on combining a standard homogeneous manganite state with a cuprate.

Thus, the electron-phonon (e-ph) interaction, crucial to understand the CMR effect, is here neglected for simplicity. In fact, LSMO does not have a large CMR effect, thus the e-ph coupling may not be strong in this material. (2) More severe is the approximation carried out on the cuprate side since a mean-field approximation with an explicitly attractive force is employed. However, this approximation will be relaxed below and the Hubbard model will be used without an explicit attraction, at the price of having to constraint the study to smaller systems than those that can be analyzed in the static mean-field approximation.

To treat the many-body interactions described by $H_I^{(R)}$, here a simple mean-field approximation is adopted. For the first interaction term, the following replacement is introduced,

$$U \sum_{\mathbf{i}} n_{\mathbf{i}\uparrow} n_{\mathbf{i}\downarrow} \rightarrow U \sum_{\mathbf{i}} [\langle n_{\mathbf{i}\uparrow} \rangle n_{\mathbf{i}\downarrow} + n_{\mathbf{i}\uparrow} \langle n_{\mathbf{i}\downarrow} \rangle - \langle n_{\mathbf{i}\uparrow} \rangle \langle n_{\mathbf{i}\downarrow} \rangle].$$

For the second term, a standard BCS model approximation is used:

$$V \sum_{\langle \mathbf{ij} \rangle} n_{\mathbf{i}} n_{\mathbf{j}} \rightarrow V \sum_{\langle \mathbf{ij} \rangle} \left[\left(\Delta_{\mathbf{ij}} c_{\mathbf{i}\uparrow}^\dagger c_{\mathbf{j}\downarrow}^\dagger + \Delta_{\mathbf{ji}} c_{\mathbf{j}\uparrow}^\dagger c_{\mathbf{i}\downarrow}^\dagger \right) + \text{H.c.} + |\Delta_{\mathbf{ij}}|^2 + |\Delta_{\mathbf{ji}}|^2 \right],$$

where $\Delta_{\mathbf{ij}} = \langle c_{\mathbf{j}\downarrow} c_{\mathbf{i}\uparrow} \rangle$. The effect of V is restricted to generate in-plane superconducting correlations. To further simplify the analysis and to reduce computational efforts, two sublattices are assumed in the xy plane since it is known that this model has a tendency toward antiferromagnetism at half-filling: e.g., $\langle n_{\mathbf{i}\uparrow} \rangle = \langle n_{i_z\uparrow}^{(A)} \rangle$ and $\langle n_{i_z\uparrow}^{(B)} \rangle$ for $(-1)^{i_x+i_y} = 1$ (A-sublattice) and -1 (B-sublattice), respectively. More details can be found in [51].

To properly describe a stable junction made out of materials with different electronic densities, it is crucial to include long-range Coulomb interactions between electrons and also with the background of positive charges. In this paper, the long-range Coulomb interactions are treated within the Hartree approximation by using the following Poisson's equation [52]:

$$\nabla^2 \phi_{\mathbf{i}} = -\alpha [\langle n_{\mathbf{i}} \rangle - n_+(\mathbf{i})], \quad (4)$$

where $\alpha = e/\varepsilon a$ (ε , e , and a are the dielectric constant, electronic charge, and lattice spacing, respectively). $n_+(\mathbf{i})$ is the background positive charge density at site \mathbf{i} . In the following, e and a are set to be 1. Furthermore, $n_+(\mathbf{i})$ is kept constant to a number n_+^L (n_+^R) on the left (right) side of the system. The Poisson's equation (4) is solved numerically using symmetric discretizations in the x and y directions, and a forward discretization in the z direction, e.g., $d^2 \phi_{\mathbf{i}}/dz^2 = \phi_{\mathbf{i}+2\mathbf{z}} - 2\phi_{\mathbf{i}+\mathbf{z}} + \phi_{\mathbf{i}}$ (\mathbf{z} : unit vector in z direction). The use of the Hartree approximation here is not a severe problem: the Poisson

equation is widely considered to be a reasonable starting point to account for charge transfer, and it is much used in the study of semiconducting systems.

To mimic a ferromagnetic half-metallic ground state on the left side of the system, the localized spins $\vec{S}_{\mathbf{i}}$ are chosen to be ferromagnetically aligned, pointing into the z direction. To mimic an A-type AF state, these classical spins are chosen with the same orientation in the xy planes but opposite between adjacent planes. On the cuprate side, the mean-field Hamiltonian H_{MF} is first Fourier transformed to momentum space in the xy plane, and the resulting Bogoliubov-De Gennes equation [53] is solved numerically by diagonalizing a $(4L_x \times 4L_y)$ Hamiltonian matrix for each momentum (k_x, k_y) . The d -wave order parameter is $\Delta_d(\mathbf{i}) = \delta(\mathbf{i}, \mathbf{x}) + \delta(\mathbf{i}, -\mathbf{x}) - \delta(\mathbf{i}, \mathbf{y}) - \delta(\mathbf{i}, -\mathbf{y})$, where $\delta(\mathbf{i}, \mathbf{j}) = \langle c_{\mathbf{i}\uparrow} c_{\mathbf{j}\downarrow} - c_{\mathbf{i}\downarrow} c_{\mathbf{j}\uparrow} \rangle / 2$, and \mathbf{x} and \mathbf{y} are unit vectors in the x and y directions, respectively.

FM-SC interface: charge transfer leading to AF

The description of the numerical results starts with a qualitative reproduction of the recent experiments [19], where transfer of charge from LCMO to YBCO was found to destroy superconductivity at the interface. In Fig. 5, the case when a FM metal forms an interface with a superconducting state (as in Fig. 1(a)) is studied. The work functions and parameters are chosen such that a transfer of charge from the left to the right takes place, as shown in Fig. 5(a) where an accumulation of charge at the interface is found. The band-bending picture, which appears to be true not only for doped band insulators but also for Hubbard insulators [54], suggests that there will be a finite region where the density will be $n=1$, with the chemical potential moving across the Hubbard gap. In Fig. 5(b) the local magnetization is shown. On the left, it is FM as expected in a one-orbital manganite model away from $n=0$ or 1. On most of the right, the magnetization is zero as in a regular superconductor. However, in the interface region the magnetization develops a staggered character suggesting the presence of AF order. Thus, as expected from the mean-field formalism the density $n=1$ is associated with antiferromagnetism. Figure 5(c) shows the suppression of the superconducting order parameter at the interface. Overall, these simple results reproduce properly the experiments where it was observed that transfer of charge from a manganite LCMO to YBCO led to the suppression of superconductivity at the interface [19].

Manganite-Cuprate interface, leading to electron-doped SC

After having crudely reproduced the main qualitative aspects of previous experiments, the same formalism can

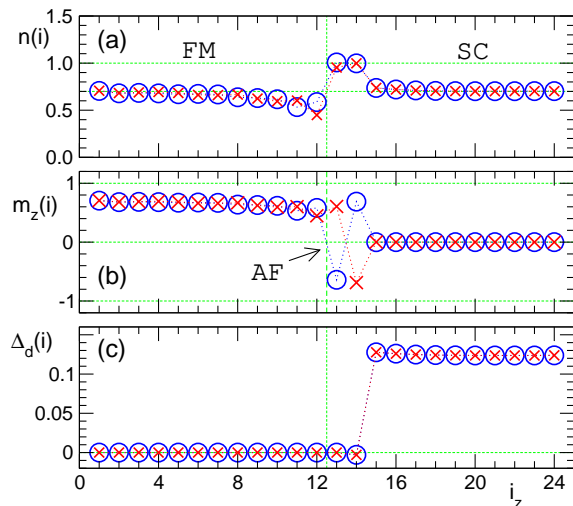


FIG. 5: (Color online) Transfer of charge from a FM half-metal to a SC state, inducing an AF interface in the process, to reproduce recent experiments [19]. Shown are the (a) electronic density n_i , (b) magnetization $m_z(\mathbf{i}) = n_{i\uparrow} - n_{i\downarrow}$, and (c) d -wave superconducting order parameter $\Delta_d(\mathbf{i})$, as a function of layer position i_z for two different sublattices $[(-1)^{i_x+i_y} = \pm 1]$ in the xy plane (denoted by circles and crosses). Here $\mathbf{i} = (i_x, i_y, i_z)$ is a lattice site position. The model parameters used are $J_H = 8t$, $t_z = t$, $W_L = 10t$, and $n_+^L = 0.7$ for the left side of the system, and $U = 4t$, $V = -3t$, $t_z = 0.1t$ (to simulate weak hopping between the Cu oxide layers), $W_R = 0$, and $n_+^R = 0.7$ for the right side of the system. $\alpha = 1$ is set for the whole system which has a size $L = 16 \times 16 \times 24$. The interface is located at $i_z = 12.5$. The localized spins in the left side of the system are fixed to be ferromagnetic. The temperature considered here is very low, $T=t/400$.

be used to formulate predictions for other systems. Of particular interest is the combination of an A-type AF state (as it occurs for instance in undoped or highly doped LSMO and also in bilayer compounds [14, 15]) and an *undoped* cuprate. If the transfer of charge occurs in the same directions as before, as already suggested by the discussion on experimental work functions, then it would be expected that at the interface a density larger than $n=1$ would be produced (see the sketch in Fig. 1(b)). If this doping is as large as 5-10%, then an electron doped superconductor could be created in a real system.

The actual calculations are conceptually simple and the results are shown in Fig. 6. In (a), the density is presented: once again a robust region in parameter space is identified where the transfer of charge occurs from the AF manganite to the AF cuprate, leading in this case to n larger than 1 at the interface. In (b), the local magnetization is shown. In this case, the G-type AF order is seen on most of the right (cuprate) region, but this magnetic order disappears at the interface due to the

transfer of charge. Finally, in (c) the superconducting order parameter is shown to become nonzero at the interface. Thus, as anticipated from the introduction, an electron-doped superconductor is predicted to occur in the manganite/cuprate system described here, within a simple mean-field approximation, for a pair of oxides with the proper location of chemical potentials.

If the A-type AF manganite state for the left side is replaced by a FM state, as before, then a similar transfer of charge occurs and within mean-field a SC state is also generated. However, it is known that the proximity-effect influence of ferromagnetism is detrimental to singlet superconductivity, thus for experimental realizations of this scenario, a non-FM state appears more suitable.

Note: if the transfer of charge would occur in the other direction, namely from the $n=1$ AF to a doped FM material, then the cuprate interface would have less charge and a narrow layer with the properties of a *hole-doped* cuprate could be expected. Thus, the simple motive of this effort works both ways at the mean-field level. However, the analysis of work functions from the experimental viewpoint, already discussed, suggests that in order to generate interfacial superconductivity involving a manganite, electron doping is the most likely outcome since the chemical potential of LSMO is above that of LCO, NCO, SCO, and YBCO.

SC at BI-AF and Metal-AF interfaces

The generation of a superconductor via transfer of charge from another compound is certainly not restricted to occur only when LSMO is involved, but it should happen under far more general circumstances. For instance, the case of a band-insulator (BI) forming an interface with an AF was also studied. Figure 7(a) shows the density profile, indicating that the parameters of the calculation are such that the transfer of charge this time occurs from the AF to the BI, inducing a region in the cuprate with hole doping, and concomitant superconductivity (as shown in (b)). Certainly, electron-doped SC can be induced as well by adjusting the work functions.

If instead of a BI, a standard metal is used (modeled in our study by merely using Hubbard $U=0$ in a tight-binding model), then for appropriate work functions also a charge transfer is to be expected (see (c) and (d)). Thus, the most important aspect of the problem is to identify materials with the proper relative location of work functions such that the charge transfer occurs in the proper direction, and also such that there is a good matching between lattice spacings to avoid generating extra complications for the transfer of charge to occur.

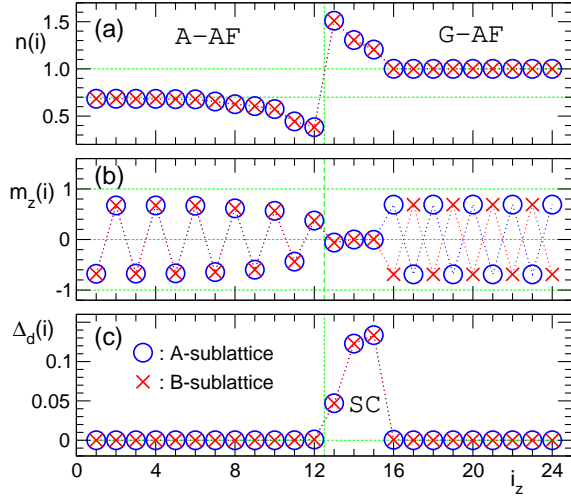


FIG. 6: (Color online) Transfer of charge from an A-type AF state (as it occurs in some doped manganites [14]) to an AF insulator (LCO, SCO, NCO, or YBCO), inducing an electron-doped SC state at the interface. The actual model parameters used here are $J_H = 8t$, $t_z = t$, $W_L = 14t$, and $n_+^L = 0.7$ for the left side of the system, and $U = 4t$, $V = -3t$, $t_z = 0.1t$, $W_R = 0$, and $n_+^R = 1.0$ for the right side of the system. $\alpha = 1$ is set for the whole system, with $L = 16 \times 16 \times 24$ being the lattice studied. The interface is located at $i_z = 12.5$. The localized spins in the left side of the systems are fixed to be antiferromagnetic in an A-type state, and the temperature of the study was $T=t/400$.

EXTENDED DYNAMICAL MEAN FIELD THEORY RESULTS FOR HUBBARD MODEL INTERFACES

To place our findings on a firmer footing, we describe here the results obtained from cluster dynamical mean field theory (CDMFT) [55] generalized to a layered geometry for the case of a ferromagnetic – Mott insulator interface. The previous section showed that there are many similarities in the use of FM or AF manganites in the heterostructure, since their main role is the donation of carriers to the cuprate. Since technically the case of FM is simpler, in this section we focus on a FM manganite. CDMFT is a powerful technique which maps a full many-body problem onto that of a cluster embedded in a self-consistent medium. The model Hamiltonian considered here is identical to Eqs. 1 and 2, with the addition of the local Coulomb interaction represented by the Hubbard U on the Mott insulating side of the interface (and without the explicitly attractive nearest-neighbors attraction). Long-range Coulomb interactions are treated again using the Poisson equation as in Eq. 4.

CDMFT can be generalized to treat the effects of a layered geometry in the same manner as DMFT was adapted to treat a film geometry [5, 56]. Each layer is

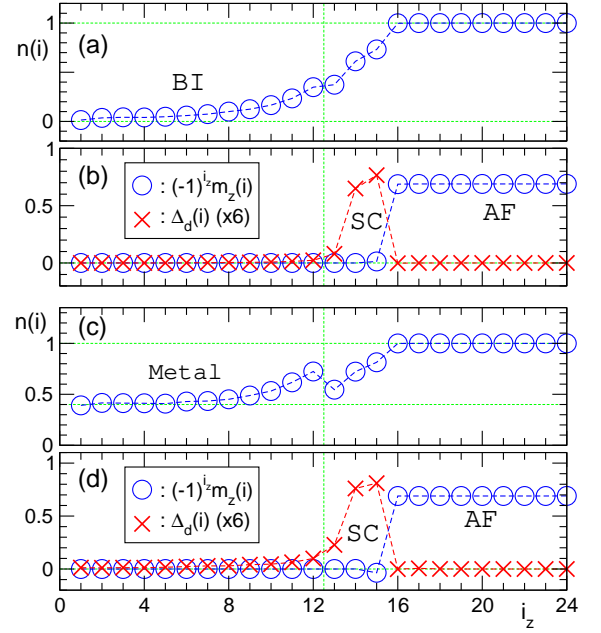


FIG. 7: (Color online) Generation of a SC state at the interface between a band insulator (BI) and an AF insulator and also between a standard metal and an AF. As in other figures, shown are the electron density n_i [(a) and (c)], and staggered magnetization $(-1)^{i_z} m_z(i)$ and d -wave superconducting order parameter $\Delta_d(i)$ [(b) and (d)] as a function of layer position i_z . The model parameters used in (a) and (b) are $J_H = 0$ (to avoid ferromagnetism), $t_z = t$, $W_L = 0$, and $n_+^L = 0.0$ (to get a crude band insulator) for the left side of the system, and $U = 4t$, $V = -3t$, $t_z = 0.1t$, $W_R = 0$, and $n_+^R = 1.0$ for the right side of the system. The same parameters are used in (c) and (d) except $n_+^L = 0.4$ for the left side of the system. $\alpha = 1$ is set for the whole system with $L = 16 \times 16 \times 24$ being the lattice studied, and the interface is located at $i_z = 12.5$.

mapped onto an independent cluster impurity embedded in a medium. The solution for the self-energy of each layer is then used via a self-consistency condition to obtain the local Green's function of the entire lattice. Hopping between the layers is taken into account only at the level of the self-consistency condition. To make the problem computationally feasible, we fix the number of layers to $L_{FM} = 5$ and $L_{MI} = 5$ for the ferromagnet and the Mott insulator, respectively. Further, each layer is mapped to a 4-site cluster embedded in a bath of 8 sites. SC correlations are included in the bath around the MI layers to allow for the SC instability and a paramagnetic solution is imposed. Individual layers are oriented in the xy -plane and stacked in the z -direction. The algorithm starts by making an initial guess for the local chemical potential and the bath parameters across the layered structure. Solving the cluster impurity model in each layer using the Lanczos method we obtain the cluster Green's function, cluster density, and self-energy.

The density in each layer is used to obtain the new local potential ϕ_z using the Poisson equation (Eq. 4). The self-energy in each layer is used to obtain a local Green's function for the lattice using the equation below:

$$G_{\text{loc}}(z, \omega) = \int \frac{dK_x dK_y}{\pi^2} G(z, z', K_x, K_y, \omega) \quad (5)$$

where

$$G(z, z', K_x, K_y, \omega) = [\omega + \mu_z - t(K_x, K_y, z, z') - \Sigma(z, z', K_x, K_y, \omega)]^{-1}. \quad (6)$$

Here, $t(K_x, K_y, z, z')$ denotes the Fourier transform of the hopping matrix (both intralayer and interlayer), K_x and K_y denote the superlattice momenta within each layer, and z denotes the layer index. μ_z includes all the terms that couple to the density, including the chemical potential, ϕ_z , site potential, and the work function on either side of the interface. The Green's function $G_{\text{loc}}(z, \omega)$ is combined with the Dyson equation to give a new Weiss field that is then used to obtain a new set of bath parameters using a conjugate gradient minimization. Convergence is achieved when the bath parameters for each layer and the density profile across the layers do not change with further iterations.

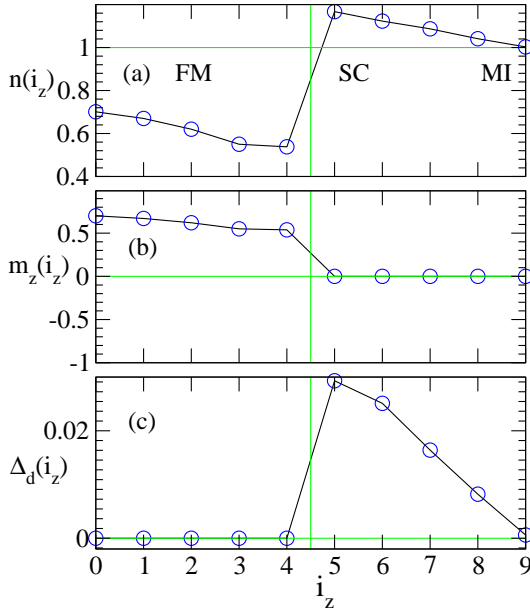


FIG. 8: Transfer of charge from a FM manganite to a Mott insulating cuprate inducing a d -wave SC state at the interface in a 10-layer heterostructure, obtained using CDMFT generalized to a layered geometry. (a) is the electronic density profile n_z ; (b) is the magnetic moment in each layer z , denote by $m_z(i_z)$; and (c) is the d -wave SC order parameter, $\Delta_d(i_z) = \langle c_{z,i\uparrow} c_{z,i+x\downarrow} \rangle$ across the heterostructure. The model parameters used are $J_H = 8t$, $t_z = t$, $W_L = 12t$, $n_+^L = 0.7$, $n_+^R = 1.0$, $W_R = 0$, $\alpha = 1$, and $U/t=8$.

In Fig. 8(a) the density profile is presented. The bulk density is at $n=0.7$ on the left side (Mn oxide) and $n=1.0$

on the right (Cu oxide, $U/t=8$). As expected from the previous discussions, electron doping of the Mott insulator occurs at the interface due to a transfer of charge from the manganite to the cuprate. Figure 8(b) provides the magnetization at each layer. Note that the effects of penetration of the FM moment onto the Mott insulator side are not considered in this calculation. In a real setup, it is likely that a finite polarization will be found on the right hand side of the figure. Figure 8(c) shows the d -wave SC order parameter, which in this heterostructure becomes non-zero in the cuprate's interfacial region and decays rapidly into the bulk of the Mott insulator. Thus, an electron-doped d -wave superconductor can be realized at the interface of a manganite and a cuprate, due to the expected transfer of charge between them, even when dynamical effects in the mean-field approximation are taken into account.

DISCUSSION AND SUMMARY

In this manuscript, the possible charge transfer from a manganite to an undoped cuprate was discussed in the context of oxide heterostructures. This issue is nontrivial since *a priori* the existence of a robust gap in the undoped Cu oxides would have suggested the lack of available states for manganite electrons to pour into the antiferromagnetic cuprates near the interfaces. The recently discovered *indirect* nature of the Cu-oxides gaps effectively reduces the magnitude of the Hubbard gap. Taking this into consideration, our analysis suggests that the Fermi level of manganites, in a robust range of hole doping, lies above the chemical potential of several cuprates and even above the bottom of the upper Hubbard band of SCO and NCO. This opens the possibility of electron doping of high- T_c 's at interfaces with manganites (and other oxides). Under idealized conditions, the doping discussed here may induce a superconducting state (if the manganite is not ferromagnetic), an exotic metallic state containing polarized carriers in an antiferromagnetic background (if the manganite is ferromagnetic), or still a superconducting state, likely with a triplet component, if the spin polarization of the carriers coming from the manganite is only partial.

An important component of our effort is the introduction of a systematic procedure to analyze photoemission and diffusion voltage experiments to predict the direction of flow of charge at interfaces. A figure with the relative Fermi levels and gap locations of several oxides was presented.

If the superconducting state is ever realized in clean interfaces, a fundamental issue to address is the unveiling of the phase diagram of cuprates in the absence of quenched disorder. This is true for both electron and hole doping. Recent phenomenological calculations [51] involving noninteracting carriers in interaction with the

AF and SC order parameters (an extension of the traditional Landau-Ginzburg approach) suggest that these phases should be separated by either a region of local coexistence or a first-order transition. A glassy state, as in the widely studied phase diagram of LSCO, was reproduced *only* incorporating quenched disorder. For a sketch of these diagrams see Fig. 9. The generation of superconductivity at interfaces may reveal the true phase diagram of clean cuprates.

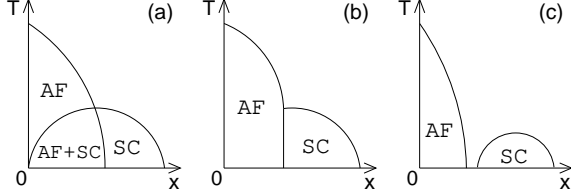


FIG. 9: (a) and (b) are the possible phase diagrams of the cuprates in the clean limit [51], which may be experimentally realized at the interfaces discussed in this paper. No distinction is made between hole or electron doping, x represents both. (c) is the well-known phase diagram of chemically doped LSCO. According to Ref. [51], the glassy state between AF and SC phases is caused by quenched disorder.

It is clear that our calculations can only be considered as suggestive, and its main purpose is to induce further work in this area. Important simplifications employed in the study, including the neglect of lattice reconstructions, vacancies, and polarity effects, need to be addressed. *Ab initio* calculations are crucial to clarify these issues. And, of course, the experimental realization of the interfaces discussed here would provide a definitive answer to the proposal of electron doping of cuprates at the interfaces.

ACKNOWLEDGMENT

We thank I. Bozovic, H. Y. Hwang, M. Kawasaki, T. Kopp, H. Kumigashira, S. Pennycook, A. Sawa, Y. Tokura, and M. Varela for valuable discussions. This work was supported in part by the NSF grant DMR-0443144 and by the Division of Materials Sciences and Engineering, Office of Basic Energy Sciences, U.S. Department of Energy, under contract DE-AC05-00OR22725 with Oak Ridge National Laboratory, managed and operated by UT-Battelle, LLC. Support by the LDRD program at ORNL is also acknowledged.

[1] A. Ohtomo, D. A. Muller, J. L. Grazul, and H. Y. Hwang, *Nature* **419**, 378 (2002).
[2] A. Ohtomo and H. Y. Hwang, *Nature* **427**, 423 (2004).
[3] S. Okamoto and A. Millis, *Nature* **428**, 630 (2004).

[4] S. Okamoto and A. J. Millis, *Phys. Rev. B* **70**, 075101 (2004).
[5] S. Okamoto and A. J. Millis, *Phys. Rev. B* **70**, 241104(R) (2004).
[6] N. Nakagawa, H. Y. Hwang, and D. A. Muller, *Nature Materials* **5**, 204 (2006), and references therein.
[7] S. Thiel, G. Hammerl, A. Schmehl, C. W. Schneider, and J. Mannhart, *Science* **313**, 1942 (2006), and references therein.
[8] E. Dagotto, *Science* **309**, 257 (2005), and references therein.
[9] A. F. Volkov, F. S. Bergeret and K. B. Efetov, *Phys. Rev. Lett.* **90**, 117006 (2003). See also N. Yoshida, M. Fogelstrom, *cond-mat/0511009*.
[10] M. Eschrig, J. Kopu, J. C. Cuevas, and Gerd Schon, *Phys. Rev. Lett.* **90**, 137003 (2003).
[11] T. Kontos, M. Aprili, J. Lesueur, F. Genet, B. Stephanidis, and R. Boursier, *Phys. Rev. Lett.* **89**, 137007 (2002).
[12] V. A. Vas'ko, V. A. Larkin, P. A. Kraus, K. R. Nikolaev, D. E. Grupp, C. A. Nordman, and A. M. Goldman, *Phys. Rev. Lett.* **78**, 1134 (1997).
[13] C. A. R. Sa de Melo, *Phys. Rev. Lett.* **79**, 1933 (1997).
[14] E. Dagotto, T. Hotta, and A. Moreo, *Physics Reports* **344**, 1 (2001).
[15] E. Dagotto, *Nanoscale Phase Separation and Colossal Magnetoresistance*, Springer (2002).
[16] J. Mannhart, D. G. Schlom, J. G. Bednorz, and K. A. Muller, *Phys. Rev. Lett.* **67**, 2099 (1991).
[17] C. H. Ahn, S. Gariglio, P. Paruch, T. Tybell, L. Antognazza, and J.-M. Triscone, *Science* **284**, 1152 (1999).
[18] For recent work in this area see N. Pavlenko, I. Elfimov, T. Kopp, and G. A. Sawatzky, *cond-mat/0605589*, and references therein. For related literature see: V. Koerting, Q. Yuan, P.J. Hirschfeld, T. Kopp, and J. Mannhart, *Phys. Rev. B* **71**, 104510 (2005); N. Pavlenko and T. Kopp, *Phys. Rev. B* **72**, 174516 (2005).
[19] M. Varela, A.R. Lupini, V. Peña, Z. Sefrioui, I. Arslan, N.D. Browning, J. Santamaria, S.J. Pennycook, *cond-mat/0508564*; see also Todd Holden, H.-U. Habermeier, G. Cristiani, A. Golnik, A. Boris, A. Pimenov, J. Humlicek, O. I. Lebedev, G. Van Tendeloo, B. Keimer, and C. Bernhard, *Phys. Rev. B* **69**, 064505 (2004); A. Hoffmann, S. G. E. te Velthuis, Z. Sefrioui, J. Santamaria, M. R. Fitzsimmons, S. Park, and M. Varela, *Phys. Rev. B* **72**, 140407(R) (2005); V. Peña, C. Visani, J. Garcia-Barriocanal, D. Arias, Z. Sefrioui, C. Leon, J. Santamaria, and C. A. Almasan, *Phys. Rev. B* **73**, 104513 (2006).
[20] H. Hilgenkamp and J. Mannhart, *Rev. Mod. Phys.* **74**, 485 (2002); and references therein. See also B. Nikolic, J. K. Freericks, and P. Miller, *Phys. Rev. B* **65**, 064529 (2002); U. Schwingenschlogl and C. Schuster, *cond-mat/0702098*.
[21] Z. Sefrioui, D. Arias, V. Peña, J. E. Villegas, M. Varela, P. Prieto, C. León, J. L. Martinez, and J. Santamaria, *Phys. Rev. B* **67**, 214511 (2003). See also V. Peña, Z. Sefrioui, D. Arias, C. León, J. Santamaria, J. L. Martinez, S. G. E. te Velthuis, and A. Hoffmann, *Phys. Rev. Lett.* **94**, 057002 (2005); J. Chakhalian, J. W. Freeland, G. Srajer, J. Strempfer, G. Khaliullin, J. C. Cezar, T. Charlton, R. Dalgliesh, C. Bernhard, G. Cristiani, H.-U. Habermeier, and B. Keimer, *Nature Physics* **2**, 244 (2006).
[22] The hole doping of an undoped cuprate when in combi-

- nation with STO has already been reported in S. Oh, M. Warusawithana, and J. N. Eckstein, Phys. Rev. B **70**, 064509 (2004). See also J. N. Eckstein and I. Bozovic, Annu. Rev. Mater. Sci. **25**, 679 (1995); G. Yu. Logvenov, A. Sawa, C. W. Schneider and J. Mannhart, App. Phys. Lett. **83**, 3528 (2003); and references therein.
- [23] L. Brey, cond-mat/0611594, and references therein.
- [24] K. Schulte, M. A. James, L. H. Tjeng, P. G. Steeneken, G. A. Sawatzky, R. Suryanarayanan, G. Dhalenne, and A. Revcolevschi, Phys. Rev. B **64**, 134428 (2001).
- [25] M. Suzuki, Phys. Rev. B **39**, 2312 (1989).
- [26] A. Ino, C. Kim, M. Nakamura, T. Yoshida, T. Mizokawa, Z.-X. Shen, A. Fujimori, T. Kakeshita, H. Eisaki, and S. Uchida, Phys. Rev. B **62**, 4137 (2000).
- [27] O. Rösch, O. Gunnarsson, X. J. Zhou, T. Yoshida, T. Sasagawa, A. Fujimori, Z. Hussain, Z.-X. Shen, and S. Uchida, Phys. Rev. Lett. **95**, 227002 (2005).
- [28] J. W. Allen, C. G. Olson, M. B. Maple, J.-S. Kang, L. Z. Liu, J.-H. Park, R. O. Anderson, W. P. Ellis, J. T. Markert, Y. Dalichaouch, and R. Liu, Phys. Rev. Lett. **64**, 595 (1990).
- [29] H. Namatame, A. Fujimori, Y. Tokura, M. Nakamura, K. Yamaguchi, A. Misu, H. Matsubara, S. Suga, H. Eisaki, T. Ito, H. Takagi, and S. Uchida, Phys. Rev. B **41**, 7205 (1990).
- [30] Note that the chemical potential difference between LCO and NCO is still controversial. Other estimations arrive to a value ~ 1 eV for this quantity. See P. G. Steeneken, L. H. Tjeng, G. A. Sawatzky, A. Tanaka, O. Tjernberg, G. Ghiringhelli, N. B. Brookes, A. A. Nugroho, and A. A. Menovsky, Phys. Rev. Lett. **90**, 247005 (2003).
- [31] A. Fujimori, A. Ino, J. Matsuno, T. Yoshida, K. Tanaka, and T. Mizokawa, J. Electr. Spectrosc. Relat. Phenom. **124**, 127 (2002).
- [32] S. Tajima, H. Ishii, T. Nakamura, H. Takagi, S. Uchida, M. Seki, S. Suga, Y. Hidaka, M. Suzuki, T. Murakami, K. Oka, and H. Unoki, J. Opt. Soc. Am. B **6**, 475 (1989).
- [33] K. Tsutsui, T. Tohyama, and S. Maekawa, Phys. Rev. Lett. **83**, 3705 (1999).
- [34] M. Z. Hasan, E. D. Isaacs, Z.-X. Shen, L. L. Miller, K. Tsutsui, T. Tohyama, and S. Maekawa, Science **288**, 1811 (2000).
- [35] A. Fujimori, A. Ino, T. Mizokawa, C. Kim, Z.-X. Shen, T. Sasagawa, T. Kimura, K. Kishio, M. Takaba, K. Tamasaku, H. Eisaki and S. Uchida, J. Phys. Chem. Solids **59**, 1892 (1998).
- [36] Y. Muraoka, T. Muramatsu, J. Yamaura, and Z. Hiroi, Appl. Phys. Lett. **85**, 2950 (2004).
- [37] M. Nakamura, A. Sawa, H. Sato, H. Akoh, M. Kawasaki, and Y. Tokura, Phys. Rev. B **75**, 155103 (2007).
- [38] T. Fujii, M. Kawasaki, A. Sawa, Y. Kawazoe, H. Akoh, and Y. Tokura, Phys. Rev. B (2007), in press.
- [39] T. Muramatsu, Y. Muraoka, and Z. Hiroi, Jpn. J. Appl. Phys. **44**, 7367 (2005).
- [40] J. Matsuno, A. Fujimori, Y. Takeda and M. Takano, Europhys. Lett. **59**, 252 (2002).
- [41] A. Ino, T. Mizokawa, A. Fujimori, K. Tamasaku, H. Eisaki, S. Uchida, T. Kimura, T. Sasagawa, and K. Kishio, Phys. Rev. Lett. **79**, 2101 (1997).
- [42] N. Harima, A. Fujimori, T. Sugaya, and I. Terasaki, Phys. Rev. B **67**, 172501 (2003).
- [43] H. Yagi, T. Yoshida, A. Fujimori, Y. Kohsaka, M. Misawa, T. Sasagawa, H. Takagi, M. Azuma and M. Takano, Phys. Rev. B **73**, 172503 (2006).
- [44] N. Harima, J. Matsuno, A. Fujimori, Y. Onose, Y. Taguchi, and Y. Tokura, Phys. Rev. B **64**, 220507(R) (2001).
- [45] M. P. de Jong, V. A. Dediu, C. Taliani, and W. R. Salaneck, J. Appl. Phys. **94**, 7292 (2003).
- [46] M. Minohara, I. Ohkuho, H. Kumigashira, and M. Oshima, Appl. Phys. Lett. **90**, 132123 (2007).
- [47] W. Reagor, S. Y. Lee, Y. Li, and Q. X. Jia, J. Appl. Phys. **95**, 7971 (2004).
- [48] The work function of YBCO has been experimentally measured. According to T. Hirano, M. Ueda, K. Matsui, T. Fujii, K. Sakuta, and T. Kobayashi, Jpn. J. Appl. Phys. **31**, L1345 (1992), the YBCO work function is 6.1 eV. Since the work function of LSMO is ~ 4.8 eV [45, 46, 47], their difference is 1.3 eV, which is not too different (given the uncertainties in these experimental results) from the numbers deduced from Fig. 3.
- [49] Are there other transition-metal oxides that can replace manganites in this context? Consider first the case of ruthenates. In addition to the $3d$ oxides, clearly the $4d$ transition-metal oxides are another potentially important class of materials for our purposes. Among them, SrRuO₃ (SRO) is known to be highly conductive and, therefore, a potential candidate for electrode in transition-metal based devices. However, through permittivity measurements, the work function of (001) SRO is estimated to be 5.2 eV (see X. Fang and T. Kobayashi, Appl. Phys. A **69**, S587 (1999)). This SRO work function is rather large compared with the value ~ 3.5 eV of the double-layered La_{1.2}Sr_{1.8}Mn₂O₇ and ~ 4.8 of the cubic perovskite LSMO [46]. This may indicate the following trend: the larger the atomic number of the transition-metal is, the larger the work function becomes. In other words, if one wants to inject electrons to some material, one may need to use transition-metal oxides with *smaller* atomic number than manganites (since reducing the atomic number also reduces the electro-negativity). From this point of view, electron-rich titanates (via the addition of Nb) can provide another route for electron doping of cuprate parent compounds, as very recently experimentally reported [37]. Our study is by no means restricted to manganites as electron donors.
- [50] E. Dagotto, J. Riera, Y. C. Chen, A. Moreo, A. Nazarenko, F. Alcaraz, and F. Ortolani, Phys. Rev. B **49**, 3548 (1994); and references therein. See also R. Micnas, J. Ranninger, and S. Robaszkiewicz, Rev. Mod. Phys. **62**, 113 (1990); I. Martin, G. Ortiz, A. V. Balatsky, and A. R. Bishop, Int. J. of Mod. Phys. **14**, 3567 (2000).
- [51] G. Alvarez, M. Mayr, A. Moreo, and E. Dagotto, Phys. Rev. B **71**, 014514 (2005). See also M. Mayr, G. Alvarez, A. Moreo, and E. Dagotto, Phys. Rev. B **73**, 014509 (2006).
- [52] See, for example, S. Datta, *Electronic transport in mesoscopic systems* (Cambridge University Press, Cambridge, 1997).
- [53] See, e.g., P. G. De Gennes *Superconductivity of Metals and Alloys* (Perseus Books, New York, 1999).
- [54] T. Oka and N. Nagaosa, Phys. Rev. Lett. **95**, 266403 (2005).
- [55] G. Kotliar, S. Y. Savrasov, G. Palsson, and G. Biroli, Phys. Rev. Lett. **87**, 186401 (2001).
- [56] M. Potthoff and W. Nolting, Phys. Rev. B **59**, 2549; **60**, 7834 (1999); S. Schwieger, M. Potthoff, and W. Nolting, Phys. Rev. B **67**, 165408 (2003).